INSTITUTE OF PHYSICS PUBLISHING JOURNAL OF PHYSICS G: NUCLEAR AND PARTICLE PHYSICS

J. Phys. G: Nucl. Part. Phys. **28** (2002) 2993–3006 PII: S0954-3899(02)54753-8

g factor measurements of μs isomeric states in neutron-rich nuclei around ^{68}Ni produced in projectile-fragmentation reactions

G Georgiev[1,2], G Neyens[1,2], M Hass[3], D L Balabanski[4,5], C Bingham[4], C Borcea[6], N Coulier[2], R Coussement[2], J M Daugas[1,2], G De France[1], F de Oliveira Santos[1], M Górska[7], H Grawe[7], R Grzywacz[4,8], M Lewitowicz[1], H Mach[9], I Matea[1,6], R D Page[10], M Pfützner[8], Yu E Penionzhkevich[11], Z Podolyák[12], P H Regan[12], K Rykaczewski[13], M Sawicka[8], N A Smirnova[1,2], Yu G Sobolev[11], M Stanoiu[1], S Teughels[2] and K Vyvey[2]

[1] GANIL, BP 55027, F-14076 Caen Cedex 5, France
[2] University of Leuven, IKS, Celestijnenlaan 200 D, B-3001 Leuven, Belgium
[3] Faculty of Physics, The Weizmann Institute of Science, 76100 Rehovot, Israel
[4] Department of Physics and Astronomy, University of Tennessee, Knoxville, TN 37996, USA
[5] Faculty of Physics, St. Kliment Ohridski University of Sofia, BG-1164 Sofia, Bulgaria
[6] IFIN, PO Box MG6, 76900 Bucharest-Magurele, Romania
[7] Gesellschaft für Schwerionenforschung mbH, D-64291 Darmstadt, Germany
[8] IEP, Warsaw University, Hoża 69, PL-00681 Warsaw, Poland
[9] Department of Radiation Sciences, ISV, Uppsala University, S-61182 Nyköping, Sweden
[10] Oliver Lodge Laboratory, University of Liverpool, Liverpool L69 7ZE, UK
[11] FLNR-JINR, Department of Physics, 141980 Dubna, Moscow Region, Russia
[12] Department of Physics, University of Surrey, Guildford, GU2 5XH, UK
[13] Oak Ridge National Laboratory, Physics Division, Oak Ridge, TN 37830, USA

Received 9 October 2002
Published 12 November 2002
Online at stacks.iop.org/JPhysG/28/2993

Abstract

We report the first g factor measurement on microsecond isomers of neutron-rich nuclei produced in projectile-fragmentation reactions at intermediate energies. The nuclides in the vicinity of ^{68}Ni were produced and spin oriented following the fragmentation of a ^{76}Ge, 61.4 MeV u^{-1} beam at GANIL. The LISE spectrometer was used to select the nuclei of interest. The time-dependent perturbed angular distribution (TDPAD) method was applied in combination with the heavy-ion–gamma correlation technique to measure the g factors of ^{69m}Cu ($J^\pi = 13/2^+$, $T_{1/2} = 350$ ns) and ^{67m}Ni ($J^\pi = 9/2^+$, $T_{1/2} = 13.3\,\mu$s). Specific details of the experimental technique and the comparison of the results ($|g(^{69m}\mathrm{Cu})| = 0.225(25)$ and $|g(^{67m}\mathrm{Ni})| = 0.125(6)$) with theoretical calculations are discussed. These results provide another indication of the importance of proton excitations across the $Z = 28$ shell gap.

1. Introduction

Magnetic moments are very sensitive probes of the detailed composition of the nuclear wavefunction. Due to their dependence on the isospin, spin and orbital angular momentum of the involved valence nucleons, they are rigorous probes for the spin/parity assignment and proton–neutron character of the nuclear states and they also serve as a stringent test of the nuclear theory.

In recent years, due to the rapid developments in the radioactive ion beam facilities and the nuclear detection techniques, a large variety of nuclear species are available for investigation. The efforts nowadays are directed towards nuclear states at the extremes of the spin, isospin and mass. From an experimental point of view, neutron-rich nuclei present a particular challenge because they are difficult or impossible to produce in the widely used fusion–evaporation reactions. Instead one is forced to apply other means of production such as projectile fragmentation. Utilization of a different nuclear reaction for obtaining the nuclei of interest also implies considerable changes in the measurement techniques. For example, a necessity for most of the methods of nuclear moment measurements is to have an initial polarization or an alignment of the nuclear spin ensemble. In fusion–evaporation reactions spin alignment is generated through the reaction mechanism itself. In the projectile-fragmentation reactions this turns out to be a more complex problem.

In the present work, we discuss the technical aspects of the application of the time-dependent perturbed angular distribution (TDPAD) method on isomeric states produced and oriented in projectile-fragmentation reactions and the present results of the first such measurement. In the first part we briefly review the basic principles of the method, as was developed for fusion–evaporation reactions, and consider its specific application to projectile fragments. In the second part, we present the results from the experiment and discuss the details of different approaches of the data analysis. Discussion of the results obtained and their comparison with theoretical calculations is given in the third part.

2. Time-dependent perturbed angular distribution method

2.1. In-beam measurements

The TDPAD method is based on the interaction of the magnetic moment of a spin-oriented nuclear ensemble of isomeric states with an external magnetic field B. In a semiclassical picture, this interaction causes a rotation of the spin-symmetry axis with a Larmor frequency:

$$\omega_L = -\frac{g\mu_N B}{\hbar} \tag{1}$$

where g is the nuclear gyromagnetic factor, μ_N is the nuclear magneton, B is the strength of the applied magnetic field and $\hbar$ is the Planck constant. In a typical in-beam experiment, a schematic set-up of which is shown in figure 1, one observes the time-dependent intensity of the emitted γ rays:

$$I(t, \theta, B) = I_0 \exp(-t/\tau) W(t, \theta, B). \tag{2}$$

Here τ is the mean lifetime of the nuclear state, and $W(t, \theta, B)$ is a term which represents the γ-ray angular distribution and its rotation due to the external magnetic field (more details can be found in [1, 2]):

$$W(t, \theta, B) = \sum_{k=\text{even}} A_k B_k P_k \{\cos(\theta - \omega_L t)\} \tag{3}$$

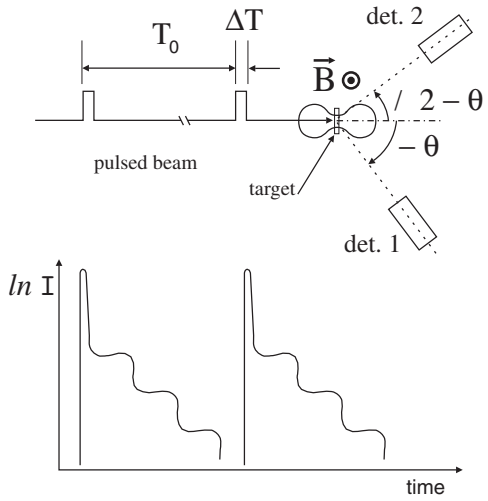

Figure 1. Typical in-beam set-up. Note that on the figure the first detector is positioned at a negative angle $(-\theta)$ and, therefore, the second detector is at $(\pi/2-\theta)$. The angles are determined with respect to the beam axis, and the magnetic field is perpendicular to the detector plane.

where A_k are the angular-distribution coefficients which depend on the multipolarity of the transition, B_k are the orientation parameters (they depend on the orientation mechanism and the spin of the nuclear state) and P_k are the Legendre polynomials. In most of the cases the product $A_k B_k$ is very small for $k \geqslant 4$ and, to a good approximation, the angular distribution is characterized by the coefficients A_2 and B_2 only. The argument of the cosine function reflects directly the fact that the nuclear ensemble has its orientation axis collinear to the beam axis.

The magnitude and the sign of the g factor can be extracted by measurements of the ratios of the intensities of γ-ray emission at two angles θ and $(\pi/2+\theta)$, respectively:

$$R(t,\theta,B) = \frac{I(t,\theta,B) - I(t,\pi/2+\theta,B)}{I(t,\theta,B) + I(t,\pi/2+\theta,B)} = \frac{3A_2B_2}{4+A_2B_2}\cos\{2(\theta-\omega_L t)\}. \tag{4}$$

Note that in the particular case of $\theta = 0$, due to the symmetry of the cosine function, the sign of the g factor cannot be extracted and the $R(t)$ function is sensitive only to its absolute value.

As is schematically shown in figure 1, the in-beam TDPAD method is usually applied on nuclear states produced by a pulsed particle beam with a period of T_0 and a pulse width of ΔT. The mean lifetime of the excited nuclear state should be shorter than the repetition time. Otherwise, the amplitude of the observed oscillations is reduced as a result of an incoherent superposition of successive decay intensities. Another requirement for these experiments is that the width of the beam pulses is much smaller than the Larmor period ($\Delta T \ll 1/\omega_L$). Thus, in an in-beam experiment one can apply the TDPAD on nuclear states with mean lifetimes in the range $\tau \sim 10^{-8}$–10^{-5} s.

2.2. Projectile-fragmentation reactions

There are several major differences between a TDPAD measurement in 'in-beam' experiments (after a fusion–evaporation reaction) and 'in-flight' (after a projectile-fragmentation reaction). The first one is related to the reaction mechanism, which causes completely different behaviour of the spin-orientation of the nuclear ensemble. The first observation of spin alignment of isomeric states in a projectile-fragmentation reaction was reported by Schmidt-Ott *et al* [3]

for ^{43m}Sc fragments from a 500 MeV u^{-1} ^{46}Ti beam. At intermediate energies, prior to the present work, spin alignment has only been utilized for moment measurements of the ground state in light nuclei [4, 5]. Although there is a schematic model, describing the dependence of the nuclear orientation as a function of the momentum distribution of the fragments [4], this subject lacks deeper understanding and needs further investigation.

In projectile-fragmentation reactions the ions, after their production, are transported through a fragment separator from the target position to the implantation host. This distance is of the order of metres, and, during the flight, the nuclei are subject to interactions with their surroundings (for example, external fields, interaction between the electron shell and the nucleus). This gives rise to the following requirements which are important for the successful application of a TDPAD measurement:

1. Only fully stripped ions should be selected by the spectrometer. Due to the interaction between the electron and the nuclear spins of the atoms, one can observe a considerable decrease up to a complete loss of the nuclear orientation, depending on the charge state of the ions [6, 7]. If the selection of fully stripped ions is not possible, one can also preserve the initial orientation in noble-gas-like charge states (see, e.g., [8]). This is an important option which needs to be considered for medium and heavy-mass nuclei, where electron pick-up processes cannot be neglected.
2. During the transport of the ions from the production target to the implantation station, the excited nuclear states are decaying. Therefore, the investigated isomeric state cannot have half-lives much shorter than the time-of-flight (TOF), which is usually of the order of a few hundred nanoseconds.
3. In the fragmentation process, the spin-aligned ensemble has its symmetry axis parallel to the primary beam direction. During the passage of the ions through the spectrometer, the orientation axis is deviated through an angle θ_L (due to the rotation of the nuclear spins with Larmor frequency), which differs from the deviation angle of the secondary beam (θ_C). This results in a misalignment between the beam direction at the implantation point and the orientation axis of the nuclear ensemble [9]:

$$\alpha = \theta_L - \theta_C = -\theta_C \left(1 - \frac{gA}{2Q}\right) \tag{5}$$

   here g is the gyromagnetic factor of the nuclear ensemble, A is the mass of the isotope in amu and Q is its charge state (equal to Z for fully stripped ions).

The angle between the secondary beam direction and the orientation axis of the nuclear ensemble results in a slight modification of equation (4) for the $R(t)$ function after a fragment separator:

$$R(t, \theta, B) = \frac{3A_2B_2}{4 + A_2B_2} \cos\{2(\theta - \alpha - \omega_L t)\}. \tag{6}$$

It is important to take this correction into account when positioning the detectors, in order to be able to determine the sign of the g factor. In the particular case when $\theta + \theta_C$ is a multiple of $\pi/2$ ($\theta + \theta_C = n \cdot \pi/2$), equation (6) can be rewritten in the form

$$R(t, (n \cdot \pi/2 - \theta_C), B) = \pm\frac{3A_2B_2}{4 + A_2B_2} \cos\left\{2g\left(\frac{\theta_C A}{2Q} - \frac{\mu_N Bt}{\hbar}\right)\right\} \tag{7}$$

where the positive sign comes for even n and the negative one is for odd n. The cosine is an even function and, therefore, the sign of the g factor cannot be determined from the $R(t)$ function.

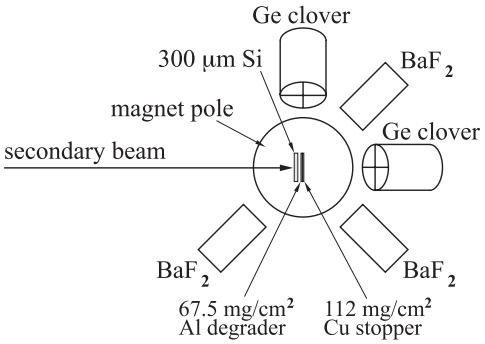

Figure 2. Schematic drawing of the set-up used during the experiment.

3. Experimental details and data analysis

Here we are reporting the results from an experiment performed at GANIL, Caen, France. Nuclei around ^{68}Ni were produced following the fragmentation of 61.4 MeV u^{-1} ^{76}Ge beam. A ^{9}Be target (145 mg cm^{-2}) was mounted on the rotating-target wheel at the entrance of the LISE separator. In a single setting of the spectrometer several isomeric states were selected. In order to decrease the flight path of the ions, and in this way to minimize their in-flight decay, we positioned our set-up at the first focal plane of LISE [10]. A 300 μm silicon energy-loss detector was used for the isotope identification using the standard energy loss versus time-of-flight (ΔE versus TOF) technique [11]. After passing through the ΔE Si detector which was also serving as a start ($t = 0$) for the time spectra, the ions were implanted into a high-purity Cu foil (112 mg cm^{-2}). The flight time between the Si detector and the Cu stopper foil was of the order of 100 ps. An Al degrader of 67.5 mg cm^{-2} was in intimate contact with the implantation host (see figure 2). No glue or other type of contact material was used between them which might result in a small gap (of the order of a μm). The Si detector, the Al degrader and the Cu foil were placed in a vacuum chamber which was positioned between the poles of an electromagnet. A static field $B = 375(7)$ mT was applied in vertical direction. The uncertainty of the magnetic field is mainly determined by its inhomogeneity over the beam spot (approximately 1×2 cm^2).

Two Ge Clover detectors [12, 13] and three BaF_2 fast scintillators were used to monitor the γ-ray intensity as a function of time. The BaF_2 scintillators, which have much better time resolution than the Ge detectors, were expected to provide valuable data. Therefore, they were set up in a configuration, from which one can determine the sign of the g factor. However, due to their inferior energy resolution, causing much lower peak-to-background ratio than for the Ge detectors, no useful results could be obtained from them. All of the results, presented below, were derived using only the data from the Ge Clover detectors.

For each of the detectors the energy and the time signals were collected in an event-by-event mode. The trigger of the data-acquisition system was provided by ions passing through the silicon ΔE detector and validated by a coincidence with a delayed γ ray, within a 17 μs time window. For an implantation rate of approximately 8000 ions s^{-1} this gave an event rate of about 800 c s^{-1}.

Several isotopes were transmitted to the implantation point after the LISE spectrometer (see figure 3). The optimization was done in a way that two of them (^{67}Ni and ^{69}Cu), with isomeric states suitable for a TDPAD measurement, were the most intensely produced. ^{67m}Ni ($J^\pi = 9/2^+$, $E_x = 1007$ keV, $t_{1/2} = 13$ μs) and ^{69m}Cu ($J^\pi = 13/2^+$, $E_x = 2741$ keV,

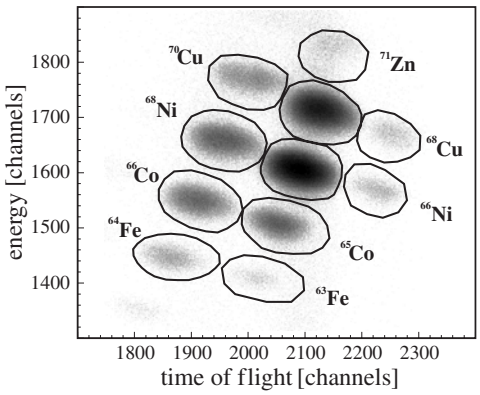

Figure 3. Typical picture of the energy-loss versus TOF spectrum. The identification of the different isotopes is also presented in the picture.

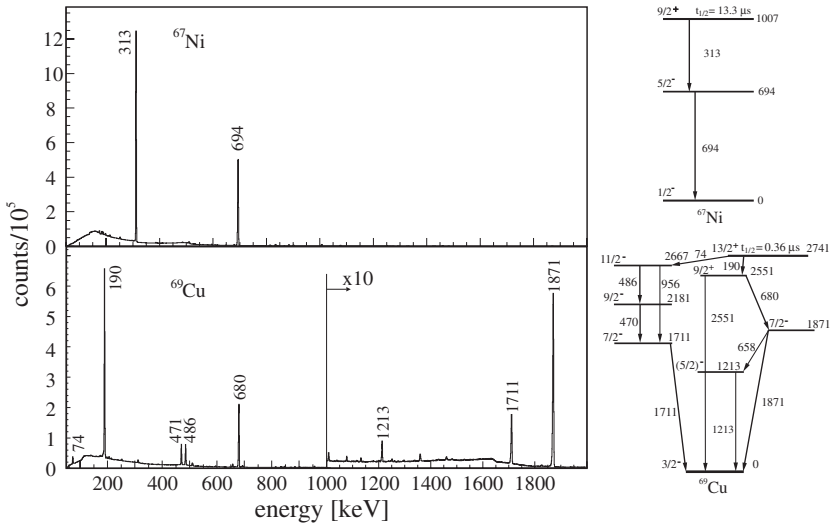

Figure 4. Energy spectra for ^{67m}Ni and ^{69m}Cu.

$t_{1/2} = 0.36$ μs) have been previously studied and their γ decay paths were known [14–17]. In our experiment we used the ΔE versus TOF identification (figure 3) to produce energy and time spectra, related to each of the implanted isotopes. The γ-ray energy spectrum which we obtained for ^{67m}Ni is presented in figure 4. The two γ lines (313 keV and 694 keV) are clearly observed. Due to the relatively short time window of our data-acquisition system, 17 μs compared to the 13.3(2) μs [16] half-life of the isomer, we could not obtain better precision on the half-life value. However, from our data we obtained $t_{1/2} = 13(1)$ μs and confirmed the quoted value within the error bar (see figure 5).

In the energy spectra, gated on the incoming ^{69}Cu ions (see figure 4), we have observed all γ transitions below the investigated isomer. This isomeric decay was previously studied in [15, 17], where the multipolarities were determined and spin/parities were assigned. Using all of the γ rays we could determine the half-life of the isomer with much higher precision (357 ± 2 ns) compared to [16].

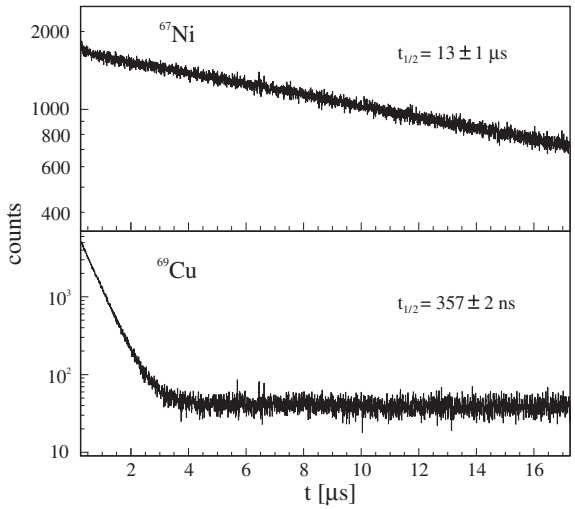

Figure 5. Time spectra for ^{67m}Ni and ^{69m}Cu. Both curves were fitted using a sum of an exponential decay plus a constant background. In the ^{69}Cu case the background was obtained directly from the time curve, while for ^{67}Ni it was estimated using the peak-to-background ratio of the energy spectrum.

The TDPAD analysis was done in two steps: first, we created time spectra for the two Ge detectors, gated on each of the isomeric γ transitions. After correcting for the difference in the efficiency we constructed the $R(t)$ function (equation (6)) as the difference between the γ-ray intensity in the first detector (positioned at 0°) and the second one ($\pi/2$), divided by their sum. Several methods of analysis were applied to the $R(t)$ functions obtained.

3.1. Direct fitting of the time-dependent oscillations

The most straightforward approach is to fit directly the $R(t)$. The effect of the fourth-order terms was neglected since in our case they contribute less than 10% to the total amplitude. Therefore equation (6) was used in the fits. There are three independent parameters in the fit, namely the amplitude of the oscillations, their frequency and their initial phase. The former one depends on the amount of the orientation of the nuclear ensemble (B_k) and on the angular-distribution coefficients (A_k) (see equation (3)). The latter two depend on the strength of the external magnetic field B and on the g factor of the nuclear state. The frequency of the oscillations can be further confirmed using the fast Fourier transform technique (see section 3.2).

The direct fit of the $R(t)$ function was done using the χ^2 minimization of the Physics Analysis Workstation package [18]. The results for the 313 keV transition in ^{67}Ni are presented in figure 6. The best fit to the data was obtained using an exponentially decaying amplitude of the oscillations ($t_{1/2} = 3.8$ μs). This can be attributed to a possible relaxation of the aligned ^{67m}Ni ensemble, implanted in the Cu host. However, due to the relatively small amplitude of the oscillations, one cannot claim high precision of the obtained relaxation time. From the fit we obtained the absolute value of the g factor of the isomeric state $|g| = 0.126 \pm 0.005$. Due to the specific positioning of our Ge detectors (see figure 2) and the total deviation angle of the secondary beam in the LISE spectrometer ($\pi/2$), we cannot determine the sign of the g factor.

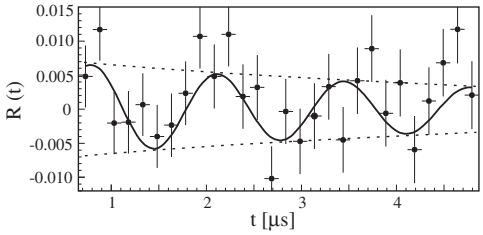

Figure 6. Direct fit of the $R(t)$ function for the 313 keV transition in ^{67}Ni. The dashed lines are eye-guides for the exponential decrease of the amplitude of the oscillations due to the relaxation effects.

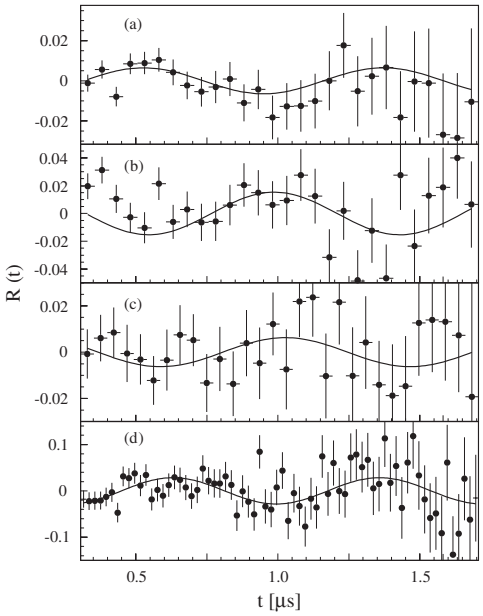

Figure 7. Direct fit of the $R(t)$ functions for the (a) 190 keV, (b) 471 keV and (c) 680 keV transitions in ^{69}Cu. The appropriate sum of three $R(t)$ functions is also presented (d).

Direct fits of the time-dependent oscillations (the $R(t)$ function) were applied to the 190 keV, 471 keV and 680 keV γ transitions in ^{69m}Cu. As was expected from the known multipolarity of the transitions [17], the amplitude of the oscillations for the 190 keV (E2) line (figure 7(a)) had opposite signs to those in the 471 keV (M1) and 680 keV (E1) transitions (figures 7(b) and (c) respectively). The $R(t)$ functions for the three transitions were summed together, taking into account their respective signs, and the result is shown in figure 7(d). The g factor which we obtained from the direct fit of the $R(t)$ function is $|g| = 0.223 \pm 0.025$.

3.2. Fast Fourier transform

The fast Fourier transform (FFT) is a method which is widely used in different approaches of data handling [19] and signal processing. It gives the transformation from the time to the frequency domain and, therefore, it can be very helpful in the analysis of a TDPAD experiment.

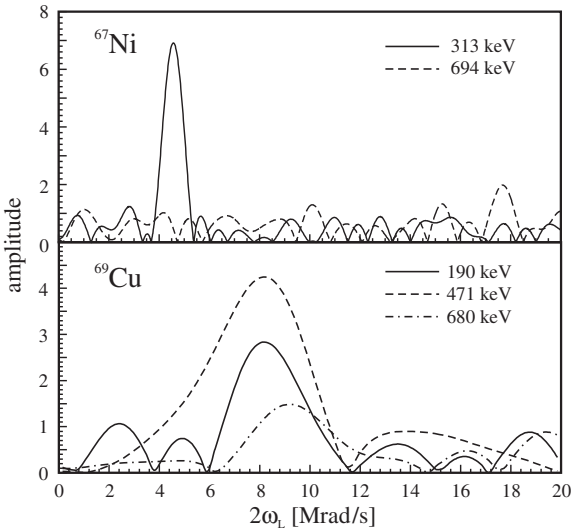

Figure 8. Results from the Fourier analysis for ^{67m}Ni and ^{69m}Cu.

In the ideal case of a g factor measurement, assuming that one observes a single-isomeric state and the nuclei are implanted in a cubic-lattice host and if there are no other perturbing interactions (e.g. quadrupole interactions), one should observe in the $R(t)$ function a single frequency, equal to the double of the Larmor frequency. However, in the more general case the feeding of the isomeric state from a higher-laying isomer, the existence of electric-field gradient in the host etc can cause the appearance of additional frequencies in the $R(t)$ function. Therefore, the FFT can be very helpful in the understanding of the data. One has to be aware that when applying the FFT on a dataset, some spurious peaks can appear due to, for example, the finite time interval and the time binning.

We applied the FFT to each of the isomeric transitions in both ^{67}Ni and ^{69}Cu. The results are presented in figure 8. Taking into account the spin-parity assignments of the isomeric, the intermediate and the ground states of ^{67}Ni (see, e.g., [16, 20, 21]), one can assume M2 and E2 characters for the 313 keV and the 694 keV transitions, respectively. A pure character of the two transitions would imply the same amplitude of the oscillations, and, therefore, the same amplitude of the peak in the FFT spectrum. However, we could observe a clear signal (see figure 8) only in the spectrum of the 313 keV line at $2\omega_L = 4.5 \pm 0.7$ Mrad s^{-1}. The error bars, here and after, are determined as the sum of the uncertainty of the position and the width of the frequency line in the FFT spectrum, obtained by a Gaussian fit. This value is very well in agreement with the results from the direct fitting of the $R(t)$ function, which gives $2\omega_L = 4.5 \pm 0.2$ Mrad s^{-1}. No signal above the background was observed in the FFT spectrum of the 694 keV transition. Although the point is disputable, this can be attributed to a possible E3 admixture in the 313 keV (M2) transition. A mixing ratio of $\delta^2 \sim 0.15$ would lead to a difference in the expected amplitude of the oscillations for the two transitions greater than 2:1.

In order to check that the signal in the 313 keV transition spectrum is not coming from any distortions due to the finite time range or the specific binning of the time spectra, we performed the FFT analysis using different time binning and different total time windows. The starting point of the application of the FFT varied between 0.5 and 1 μs and the end point was between 5 and 6 μs. In all of them the pattern of the FFT spectrum stayed the same.

Time spectra and $R(t)$ functions were produced using an energy gate just a few keV below and above the 313 keV γ line. The FFT spectra of the background did not show any signal, similar to the one of the 313 keV transition. This confirms that the observed frequency is not related to any 'contamination' in the background around the photo peak, but is associated with that precise energy of 313 keV.

In the energy spectrum, gated on the incoming ^{69}Cu ions the 313 keV γ line is also present, but it is very weak. This is caused by random coincidences due to the relatively long half-life of the ^{67}Ni isomer, which contaminates all of the γ spectra. The FFT spectrum of the 313 keV line, related to ^{69}Cu incoming ions, also did not show any peak, as expected for non-correlated events.

All of the above give us the confidence that the frequency, which we observed in the 313 keV γ line of ^{67}Ni, is indeed a real signal coming from the isomeric transition.

After the FFT analysis of the isomeric transitions of ^{69}Cu, we observed peaks in the frequency spectra of three γ lines: 190 keV (E2), 471 keV (M1) and 680 keV (E1). The results are presented in the second part of figure 8. The frequencies which we can derive from the spectra are as follow: $2\omega_L(190) = 8.3 \pm 2.3$ Mrad s^{-1}, $2\omega_L(471) = 7.9 \pm 3.3$ Mrad s^{-1} and $2\omega_L(680) = 9.3 \pm 2.6$ Mrad s^{-1}. Here the peaks are less pronounced than in the ^{67}Ni case, but their concentration at the same position (within the error bars) and their persistence for different time binning and different time windows provide the confidence in the results. The weighted mean value of the three different frequencies ($2\omega_L = 8.5 \pm 2.3$ Mrad s^{-1}) is in agreement with the direct fitting procedure, from which one can derive $2\omega_L = 8.0 \pm 0.9$ Mrad s^{-1}.

3.3. Autocorrelation analysis

The relatively long half-life of the ^{67}Ni isomeric state (13.3 μs) gave us the opportunity to test in a projectile-fragmentation experiment still another method of data handling: the autocorrelation analysis.

Since the period of the Larmor precession is much shorter than the half-life of the isomer, it is possible to fold back information of the full 17 μs window into the first $\sim$5 μs using an autocorrelation function. This method is widely used in signal processing (see, e.g., [22, 23]). Here, we will discuss only some of its main characteristics which are of importance for the present analysis.

The autocorrelation function of a dataset finds a correlation between the data at the time t and the values at a later moment $t + \tau$. In integral expression it has the form

$$X(\tau) = \lim_{T\to\infty} \frac{1}{T} \int_0^T f(t) f(t+\tau)\, \mathrm{d}t. \tag{8}$$

The quantity $X(\tau)$ is a real function with a maximum at $\tau = 0$. If the data, treated by the autocorrelation analysis, represent a harmonic function, then the autocorrelation function will have the same period as the harmonic function. Using the autocorrelation procedure one loses the phase information. Thus, for any phase of the harmonic oscillations the autocorrelation function will be a cosine function with an initial phase equal to zero. In the overall case, the amplitude of $X(\tau)$ does not coincide in any way with the amplitude of the harmonic function $f(t)$.

Since in our case we are going to deal with discrete data points, it is more convenient to transform the autocorrelation function from an integral to a discrete expression and also to normalize it:

$$X(n) = \sum_{k=k_1}^{k_2-n} \frac{f(k) f(k+n)}{k_2 - k_1 - n} \Bigg/ \sum_{k=k_1}^{k_2} \frac{f^2(k)}{k_2 - k_1}\,. \tag{9}$$

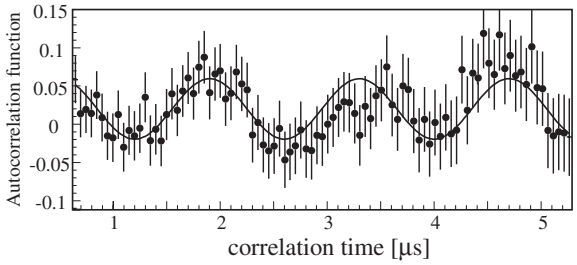

Figure 9. Autocorrelation function of the 313 keV transitions in ^{67}Ni.

Table 1. Summary of the results from the different approaches in the data analysis. The FFT result for ^{69m}Cu is obtained as an weighted mean of the three transitions. See the text for the details about the adopted values.

	Method of analysis			
	Direct fitting	FFT	Autocorrelation	Adopted value
^{67m}Ni	0.126 ± 0.005	0.125 ± 0.019	0.125 ± 0.005	0.125 ± 0.006
^{69m}Cu	0.223 ± 0.025	0.237 ± 0.064		0.225 ± 0.025

After the normalization, in the ideal case of treating a strictly harmonic function without any noise components, one should obtain a pure cosine function with an amplitude, normalized to unity, independent of the amplitude of the original function. Also, it is a general rule that the maximum value of n, in which the function is presented, should be much smaller than the full observation window $(k_2 - k_1)$.

Applying the autocorrelation analysis to the 313 keV data, we obtained the picture shown in figure 9. From the fit of the time-dependent oscillations we obtained a value for the g factor $|g| = 0.125 \pm 0.05$ in agreement with the other methods of analysis. The amplitude of the autocorrelation function is far from unity. This can be attributed to the fact that we did not observe a pure harmonic function. The amplitude of the oscillations is decreasing exponentially with $t_{1/2}$ of the order of 4 μs (see figure 6), which is about four times shorter than the total time window in which the autocorrelation analysis was performed (17 μs).

4. Results and discussion

A summary of the results from the different methods of analysis is given in table 1. As one can see, the smallest statistical error bars are obtained by the direct fitting of the $R(t)$ function using equation (6). This is due to the fact that in that fit we have one additional parameter (the initial phase of the oscillations) which depends on the isomeric g factor and which is a free parameter in the other methods of analysis. The error bars of the adopted values include the statistical errors, determined from the fits, as well as the systematic uncertainties, which mainly originate from the inhomogeneity of the external magnetic field. Knight-shift and paramagnetic corrections are negligible [24], compared to the other uncertainties.

In order to compare the measured g factors with the theoretical expectations we performed shell-model calculations in a spherical basis. In these calculations we used the S3V [25] and the modified Hjorth-Jensen *et al* [26] interactions. ^{56}Ni was considered as an inert core. The model space included $p_{3/2}$, $f_{5/2}$, $p_{1/2}$ and $g_{9/2}$ orbitals, unrestricted for ^{67}Ni and with no-more

Table 2. Theoretical values of the g factors of the two $13/2^+$ states in ^{69}Cu. Note that subscripts 1, 2 refer to opposite leading configurations in the two calculations. See the text for more details.

	S3V			Modified Hjorth-Jensen *et al* interaction	
	g^{free}	g^{eff}		g^{free}	g^{eff}
$13/2^+_1$	+0.268	+0.228	$13/2^+_1$	+0.240	+0.212
$13/2^+_2$	+0.309	+0.256	$13/2^+_2$	+0.301	+0.242

than five particles in the $g_{9/2}$ orbital for ^{69}Cu. In the g factor calculations for states with a spin J we used free proton and neutron g factors to calculate $g^{\text{free}}(J)$ or effective values $g_l^{\text{eff}} = g_l^{\text{free}}$ and $g_s^{\text{eff}} = 0.7 g_s^{\text{free}}$ to calculate $g^{\text{eff}}(J)$.

In the low-energy spectrum of ^{69}Cu, there appear two states with $J^\pi = 13/2^+$ very close in energy and within few hundred keV from the observed $13/2^+$ isomer. The wavefunctions of these states represent a mixture of many configurations. However, the principal contribution to one of these states is the $\pi p_{3/2} \otimes \nu f_{5/2}^5 g_{9/2}$ configuration, while the other state has a larger contribution from the $\pi p_{3/2} \otimes \nu p_{1/2} g_{9/2}$ configuration. The former state appears lower in energy than the latter one in the calculations using the S3V interaction, and vice versa in the calculations with the interaction of Hjorth-Jensen. The theoretical g factors of the two $13/2^+$ levels are presented in table 2.

The calculations using effective g factors reproduce much better the experimental result than those in which free-nucleon g factors are used. The calculated g factors for the two $13/2^+$ states have very similar values, mainly because the g factors for pure configurations are very similar ($g^{\text{eff}}(\pi p_{3/2} \otimes \nu f_{5/2}^5 g_{9/2}) = +0.317$ and $g^{\text{eff}}(\pi p_{3/2} \otimes \nu p_{1/2} g_{9/2}) = +0.348$). Therefore, it is not possible to claim a specific configuration for the isomeric state.

Calculations in a generalized seniority approximation have been performed by Monnoye *et al* [27] in a full $pf + g_{9/2}$ shell. In that work, the main component of the $13/2^+$ wavefunction is found to have a $\pi p_{3/2} \otimes \nu p^{-1} g$ configuration. The effective g factor of the state was calculated to be +0.241, also in agreement with our experimental value. Although this approximate approach gives a good agreement with the experimental level schemes of the less neutron-rich nuclei, the level scheme of ^{69}Cu is not well reproduced. The authors suggest that an overestimated $Z = 28$ shell gap in their interaction might cause this discrepancy [27].

The Ni isotopes have a magic proton number ($Z = 28$). Neutron number 40 was also suggested to be a new magic number far from stability [28, 29], based on the high energy of the first excited 2^+ state. From this point of view ^{67}Ni is expected to be a simple case with a single neutron hole in the 'doubly magic' ^{68}Ni core. On the other hand, there is no clear evidence for a $N = 40$ shell gap from the two-neutron separation energies S_{2n} [30] and their differences δ_{2n} [31]. This effect is well reproduced when quadrupole correlations are taken into account [32, 33]. It is also worth mentioning that the low $B(E2)$ value in ^{68}Ni [34] and the g factors of the first 2^+-excited states in a chain of Ni isotopes [35] could be reproduced only after proton excitations across the $Z = 28$ shell gap were considered.

The shell-model calculations for the g factor of the lowest $9/2^+$ state in ^{67}Ni yield $g^{\text{free}} = -0.407(-0.415)$ and $g^{\text{eff}} = -0.284(-0.290)$ using, respectively, the S3V and the modified Hjorth-Jensen *et al* interactions. The g factor obtained in the generalized seniority approach is $g^{\text{eff}} = -0.252$ [27]. All of the calculated effective g factors overestimate the measured value $|g_{\text{exp}}| = 0.125(6)$ by about a factor of 2.

At that point it was suggested [36] that a particular type of M1 excitation across the $Z = 28$ shell gap might account for the observed gyromagnetic factor. This type of configuration

mixing into the nuclear wavefunction is not taken into account in the present calculations, but does appear in the seniority approach of Monnoye *et al* [27]. A reduction of the $Z = 28$ shell gap for neutron-rich Ni nuclei (as suggested in [27, 37]) could strongly influence the g factor due to enhanced first-order corrections to the magnetic moment [38]. For example, around the doubly magic ^{208} Pb, even small contributions of $1p - 1h$ excitations across the $Z = 82$ shell gap, in particular 1^+-excitations between the $\pi\left(h_{11/2}^{-1}h_{9/2}\right)$ spin–orbit partners, strongly affect the magnetic moments [39, 40]. Such type of particle–core coupling configurations are even more favourable in the Ni isotopes, having a free $\pi f_{5/2}$ orbital just above the fully occupied $\pi f_{7/2}$ orbit. An enhancement of this first-order correction can be expected if the $Z = 28$ shell gap is reduced for the more neutron-rich isotopes. The measured gap at ^{68}Ni of 5.91(28) MeV [41] as compared to ^{56}Ni (6.47 MeV [41]) allows for a moderate reduction of the g factor only, within the large uncertainty. Note that the relevant $f_{7/2} - f_{5/2}$ gap is about 1 MeV larger in both cases. On the other hand, Pauli-blocking can reduce this core polarization effect when the orbit above the shell gap is getting filled [38], as illustrated for the $N = 126$ isotones in the Pb-region [42].

To explore the influence of core polarization in accounting for the quenching of the experimentally derived g factor of the ^{67m}Ni, we performed a two-state configuration mixing calculation in the approach of Arima and Horie [43]. We estimated the influence on the magnetic moment for a mixing between a pure $\nu g_{9/2}$ configuration and a particle–core coupled configuration $|1\rangle = \left|\pi\left(f_{7/2}^{-1}f_{5/2}\right)_{1^+} \otimes \nu g_{9/2}; 9/2^+\right\rangle$. Thus, we calculated the magnetic moment for a mixed wavefunction $|9/2^+\rangle_{\mathrm{mixed}} = a|1\rangle + \sqrt{(1-a^2)}|\nu g_{9/2}\rangle$. Taking into account only first-order effects and using free-nucleon g factors, we find that a 2% admixture of this type can explain the measured g factor of ^{67m}Ni (assuming the g factor has a negative sign).

The actual result supports the previous evidence [35] suggesting that a proton excitation across the $Z = 28$ shell gap is required in order to explain experimental data in the Ni isotopes. More investigations, both in theoretical and in experimental directions, are necessary to confirm the schematic explanation presented above.

5. Conclusions

We have shown the feasibility of applying the TDPAD method on nuclei produced and spin-aligned in projectile-fragmentation reactions. This opens up new opportunities for nuclear moment studies of neutron-rich isomeric states, not easily accessible by other conventional techniques. The results obtained show the extreme sensitivity of the magnetic moment observable to specific excitations in the nuclear wavefunction.

Acknowledgments

This work has been supported by the Access to Large Scale Facility program under the TMR programme of the EU, under contract no ERBFMGECT950036. We are grateful to the GANIL engineers for providing us the beam in stable conditions and the EXOGAM-collaboration in particular and also to the CEA (France), EPSRC (UK) and NBI (Denmark) for providing the Clover detectors. NAS is grateful to E Caurier of IReS and F Nowacki of LPT, Strasbourg, for their hospitality and kindness in allowing us to use their shell model code and for the helpful discussions. We acknowledge the discussions with P Van Isacker and O Monnoye from GANIL concerning theoretical issues of the problem. NAS and GN are post-doctoral researchers of the FWO-Vlaanderen Belgium. The WI group is partially supported by the Israel Science Foundation. Partial financial support under DOE contract DE-FG02-96ER40983 and

by the Polish Committee of Scientific Research under grant KBN 2 P03B 036 15 is also acknowledged.

References

[1] Christiansen J (ed) 1983 *Hyperfine Interactions of Radioactive Nuclei* (Berlin: Springer)
[2] Postma H and Stone N (ed) 1983 *Low-Temperature Nuclear Orientation* (Amsterdam: North-Holland)
[3] Schmidt-Ott W-D *et al* 1994 *Z. Phys.* A **350** 215
[4] Asahi K *et al* 1991 *Phys. Rev.* C **43** 456
[5] Neyens G *et al* 1997 *Phys. Lett.* B **393** 36
[6] Goldring G 1982 *Heavy Ion Collisions* ed R Bock (Amsterdam: North-Holland) p 483
[7] Vyvey K *et al* 2000 *Phys. Rev.* C **62** 034317
[8] Dafni E and Satteson M 1988 *Phys. Rev.* C **38** 2949
[9] Neyens G, Nouwen R and Coussement R 1994 *Nucl. Instrum. Methods Phys. Res.* A **340** 555
[10] Anne R *et al* 1987 *Nucl. Instrum. Methods Phys. Res.* A **257** 215
[11] Bazin D *et al* 1990 *Nucl. Phys.* A **515** 349
[12] Duchene G *et al* 1999 *Nucl. Instrum. Methods Phys. Res.* A **432** 90
[13] Shepherd S *et al* 1999 *Nucl. Instrum. Methods Phys. Res.* A **434** 373
[14] Pawlat T *et al* 1994 *Nucl. Phys.* A **574** 623
[15] Broda R *et al* 1998 Fission and properties of neutron-rich nuclei *Proc. Int. Conf. (Sanibel Island, FL, 1997)* p 202
[16] Grzywacz R *et al* 1998 *Phys. Rev. Lett.* **81** 766
[17] Ishii T *et al* 2000 *Phys. Rev. Lett.* **84** 39
[18] Physics analysis workstation package webpage http://paw.web.cern.ch/paw/
[19] Teukolsky S A, Vetterling W T and Flannery B P 1993 *Numerical Recipes (The Art of Scientific Computing)* ed W H Press (Cambridge, UK: Cambridge University Press) webpage http://www.ulib.org/webRoot/Books/Numerical_Recipes/
[20] Weissman L *et al* 1999 *Phys. Rev.* C **59** 2004
[21] Rikovska J *et al* 2000 *Phys. Rev. Lett.* **85** 1392
[22] Lange H 1967 *Correlation Techniques* (London: Iliffe Books)
[23] Bendat J S and Piersol A G 1966 *Measurement and Analysis of Random Data* (New York: Wiley)
[24] Haas H Private communication
[25] Sinatkas J, Skouras L, Strottman D and Vergados J 1992 *J. Phys. G: Nucl. Part. Phys.* **18** 1377, 1401
[26] Hjorth-Jensen M, Kuo T and Osnes E 1995 *Phys. Rep.* **261** 125 (modified by F Nowacki private communication)
[27] Monnoye O, Pittel S, Engel J, Bennett J R and Van Isacker P 2002 *Phys. Rev.* C **65** 044322
[28] Bernas M *et al* 1982 *Phys. Lett.* B **113** 279
[29] Broda R *et al* 1995 *Phys. Rev. Lett.* **74** 868
[30] Seifert H *et al* 1994 *Z. Phys.* A **349** 25
[31] Oros-Peusquens A and Mantica P 2000 *Nucl. Phys.* A **669** 81
[32] Reinhard P-G *et al* 2000 *RIKEN Rev.* **26** 23
[33] Grawe H and Lewitowicz M 2001 *Nucl. Phys.* A **693** 116
[34] Sorlin O *et al* 2002 *Phys. Rev. Lett.* **88** 092501
[35] Kenn O *et al 2001 Phys. Rev.* C **63** 021302
[36] Grawe H Private communication
[37] Franchoo S *et al* 2001 *Phys. Rev.* C **64** 054308
[38] Castel B and Towner I S 1990 *Modern Theoreis of Nuclear Moments* (Oxford: Clarendon Press)
[39] Poppelier N A F M and Glaudemans P W M 1988 *Z. Phys.* A **329** 275
[40] Stuchbery A E *et al* 1993 *Nucl. Phys.* A **555** 355
[41] Audi G and Wapstra A H 1993 *Nucl. Phys.* A **565** 1
[42] Towner I S, Khanna F C and Hausser O 1977 *Nucl. Phys.* A **277** 285
[43] Arima A and Horie H 1954 *Prog. Theor. Phys.* **12** 623